The N-terminal domain of the type 1 Ins(1,4,5)P_3 receptor stably expressed in MDCK cells interacts with myosin IIA and alters epithelial cell morphology

Michel C. Hours[1] and Laurence Mery[2,3,*]

[1]CNRS UMR 8080, 91405, Orsay, France, [2]INSERM UMRS-757, 91405, Orsay, France and [3]Université Paris-Sud, Rue Georges Clémenceau, Bâtiment 443, 91405, Orsay, France

*Author for correspondence (laurence.mery@u-psud.fr)

Accepted 25 January 2010
Journal of Cell Science 123, 1449-1459

doi:10.1242/jcs.057687

Summary

Cytosolic Ca^{2+} controls a wide range of cellular events. The versatility of this second messenger depends on its ability to form diverse spatial and temporal patterns, including waves and oscillations. Ca^{2+}-signaling patterns are thought to be determined in part by the subcellular distribution of inositol (1,4,5)-trisphosphate receptors [Ins(1,4,5)P_3Rs] but little is currently known about how the localization of the Ins(1,4,5)P_3R itself is regulated. Here, we report that the recruitment of GFP-tagged Ins(1,4,5)P_3Rs in the vicinity of tight junctions in Madin-Darby canine kidney (MDCK) cells requires the N-terminal domain. Stable expression of this domain in polarized MDCK cells induced a flattened morphology, affected cytokinesis, accelerated cell migration in response to monolayer wounding and interfered with the cortical targeting of myosin IIA. In addition, downregulation of myosin IIA in polarized MDCK cells was found to mimic the effects of stable expression of the N-terminal part of Ins(1,4,5)P_3R on cell shape and to alter localization of endogenous Ins(1,4,5)P_3Rs. Taken together, these results support a model in which the recruitment of Ins(1,4,5)P_3Rs at the apex of the lateral membrane in polarized MDCK cells, involves myosin IIA and might be important for the regulation of cortical actin dynamics.

Key words: Calcium signaling, Epithelial cells, Inositol (1,4,5)-trisphosphate receptor, Myosin II

Introduction

The intracellular second messenger, inositol (1,4,5)-trisphosphate [Ins(1,4,5)P_3 or IP_3] has a crucial role in a broad range of processes such as proliferation and differentiation, fertilization, learning and memory, apoptosis and secretion (Berridge, 1993; Mikoshiba, 1997). Ins(1,4,5)P_3 is generated upon stimulation of cell-surface receptors linked to phospholipase C (PLC) activation. It diffuses throughout the cytosol and subsequently binds to Ins(1,4,5)P_3-gated Ca^{2+} channels, primarily located in the membrane of the endoplasmic reticulum (ER). Binding of Ins(1,4,5)P_3 to its receptor initiates complex Ca^{2+} signals with widely different spatial and temporal profiles (Berridge et al., 2003). How this diversity is generated and exploited to control specific cellular functions remains a key question in the vast area of cell biology.

Three Ins(1,4,5)P_3 receptor isoforms, encoded by distinct genes and referred to as Ins(1,4,5)P_3R1, Ins(1,4,5)P_3R2 and Ins(1,4,5)P_3R3 (type 1, 2 and 3, respectively), exist in mammals. They are co-expressed in a variety of cells and can be present as homo- or heterotetramers (Joseph et al., 1995; Monkawa et al., 1995; Wojcikiewicz et al., 1995). The three isoforms share a common structure consisting of an N-terminal Ins(1,4,5)P_3-binding core, a C-terminal channel-forming domain and a central coupling or modulatory domain. However, they differ in many respects, such as modulation by small molecules (i.e. Ca^{2+} and ATP), post-translational modifications (i.e. glycosylation and phosphorylation), degradation by proteases during chronic agonist treatment and relative abundance in individual cell types (reviewed by Taylor et al., 1999). These isoform-specific differences, combined with heteromeric assembly of Ins(1,4,5)P_3R subunits, generate considerable diversity in the regulation of Ins(1,4,5)P_3R channels and could help account for the complex patterns of Ca^{2+} signals observed in vivo.

Another factor that might contribute to the heterogeneity of Ca^{2+} signals in terms of time and space is the uneven distribution of Ins(1,4,5)P_3Rs within the ER and their recruitment to specific regions of the cells. For example, in a number of epithelial cells, Ca^{2+} waves are the result of sequential Ca^{2+} release from apically segregated Ins(1,4,5)P_3R2 or Ins(1,4,5)P_3R3, followed by basolateral Ins(1,4,5)P_3R1 (Ashby and Tepikin, 2002). Despite these observations, very little is known about the molecular mechanisms that regulate Ins(1,4,5)P_3R localization. The principal factors that have been identified to date are protein 4.1N (Maximov et al., 2003; Zhang et al., 2003), which regulates the actin-dependent diffusion of Ins(1,4,5)P_3R1 in neurons (Fukatsu et al., 2004), and ankyrin B, which is required for normal Ins(1,4,5)P_3R localization in mouse neonatal cardiomyocytes and thymocytes (Tuvia et al., 1999). Both proteins directly interact with Ins(1,4,5)P_3R1 (Maximov et al., 2003; Zhang et al., 2003; Kline et al., 2008). However, 4.1N does not associate with Ins(1,4,5)P_3R2 or Ins(1,4,5)P_3R3 (Maximov et al., 2003), as determined by yeast two-hybrid screening, whereas the interaction between Ins(1,4,5)P_3R1 and ankyrin B appears to be rather cell-type specific because it does not occur in skeletal or smooth muscles (Mohler et al., 2004). Thus, other accessory proteins are likely to be involved in Ins(1,4,5)P_3R recruitment to specific subcellular locations.

A previous study indicated that the spatial distribution of endogenous Ins(1,4,5)P_3R3, as well as that of stably expressed GFP-tagged Ins(1,4,5)P_3R1, changes when MDCK cells grow from subconfluence to confluence (Colosetti et al., 2003). As cell polarity develops, Ins(1,4,5)P_3Rs are recruited in the vicinity of tight

junctions (TJ) whereas classical ER markers remain uniformly distributed throughout the cells. To further understand the molecular mechanism accounting for this localization, we expressed in MDCK cells, functional domains of Ins(1,4,5)P_3R1 with the expectation that they would interfere with endogenous receptor targeting and functions. In the present report, we demonstrate that the accumulation of Ins(1,4,5)P_3R1-GFP at the apex of the lateral membrane depends on its N-terminal region. Stable expression of the latter region in polarized MDCK cells led to abnormal localization of both endogenous Ins(1,4,5)P_3Rs and the actin-based motor myosin IIA and caused numerous phenotypic changes, including an increased number of multinucleated cells and alterations in cell shape and motility. The effects of stable expression of the Ins(1,4,5)P_3R1 N-terminal region on cell morphology and Ins(1,4,5)P_3R3 localization could be mimicked by small interfering RNA (siRNA)-mediated down-regulation of myosin IIA in polarized wild-type MDCK cells. Taken together, our results suggest that myosin IIA anchors Ins(1,4,5)P_3Rs near the TJ in polarized MDCK cells and thus, contributes to the spatial organization of Ca^{2+} signals. Conversely, Ins(1,4,5)P_3Rs could control essential processes, including morphogenesis, by regulating (at least in part) the contractility of the apical actomyosin network.

Results

The N-terminal domain is required for Ins(1,4,5)P_3R1-GFP recruitment near the TJ in polarized MDCK cells

To gain insight into the molecular mechanisms underlying Ins(1,4,5)P_3R1-GFP recruitment near the TJ as cell polarity develops, a truncated form of the Ca^{2+}-channel subunit lacking almost the entire N-terminal region (residues 79-1959) was generated and stably expressed in MDCK cells (supplementary material Fig. S1). To ensure that the so-called ΔNter-GFP mutant was still targeted to the ER, its subcellular localization was first examined in subconfluent cells, by confocal microscopy. The ER was visualized simultaneously by staining with an antibody directed against the ER-resident enzyme PDI. As shown in supplementary material Fig. S2A, ΔNter-GFP could be detected in an intricate network of tubules and vesicular structures expanding from the nuclear envelope to the cell periphery. This pattern was very similar to that of PDI and consistent with staining of the ER structure.

To determine whether the N-terminal domain is required for Ins(1,4,5)P_3R redistribution upon epithelial cell differentiation, the subcellular localization of Ins(1,4,5)P_3R1-GFP and ΔNter-GFP were next compared with that of PDI, endogenous Ins(1,4,5)P_3R3 or the TJ-associated protein ZO-1, in confluent monolayers (supplementary material Fig. S2). As previously reported (Colosetti et al., 2003), Ins(1,4,5)P_3R1-GFP was found to be mostly concentrated at the apex of the lateral membrane in proximity to ZO-1 and to co-localize with Ins(1,4,5)P_3R3 but not with PDI. By contrast, the ΔNter-GFP pattern did not overlap extensively with that of Ins(1,4,5)P_3R3 or ZO-1 but was still clearly coincident with PDI staining. Thus, unlike Ins(1,4,5)P_3R1-GFP and endogenous Ins(1,4,5)P_3R3, ΔNter-GFP remained evenly distributed in the ER in polarized cells. This result prompted us to stably express the N-terminal domain of Ins(1,4,5)P_3R1 (residues 1-2217) fused to EGFP in MDCK cells, with the expectation that this construct would interfere with endogenous Ins(1,4,5)P_3R targeting and functions.

Nter-GFP expression reduces the final cell density of MDCK monolayers without inducing apoptosis or premature exit from the cell cycle

The subcellular localization of the Nter-GFP mutant (supplementary material Fig. S1) was first investigated by indirect immunofluorescence microscopy. Three or nine days after plating, MDCK cells expressing either Ins(1,4,5)P_3R1-GFP or Nter-GFP were stained with an anti-ZO-1 antibody, to visualize cell-cell contacts. As shown in Fig. 1A, Nter-GFP was diffusely distributed throughout the cytosol at both day 3, when cells were subconfluent, and day 9, when translocation of Ins(1,4,5)P_3R1-GFP to the cell periphery has already occurred in control cells. However, as revealed by ZO-1 immunostaining, the Nter-GFP monolayer at day 9 consisted of fewer cells (Fig. 1B), suggesting that the deletion mutant interferes with epithelial cell growth.

To test this hypothesis, cell proliferation was monitored over a period of 1 week. Nter-GFP cells showed consistent reduction in cell density during the plateau phase (Fig. 2A), although Ins(1,4,5)P_3R1-GFP and Nter-GFP cells had similar doubling time during log-phase growth (15.6±0.2 hours for Ins(1,4,5)P_3R1-GFP cells versus 15.7±0.4 hours for Nter-GFP cells, n=3). To determine whether contact inhibition of cell division occurred prematurely in Nter-GFP cells, expression of PCNA, a proliferation marker, was examined over time by western blotting. As shown in Fig. 2B, after reaching confluence and during transit to the plateau phase, the amount of PCNA protein slowly decreased in cells expressing Ins(1,4,5)P_3R1-GFP (indicating that they were exiting the cell cycle), but remained elevated and steady in Nter-GFP cells. Thus,

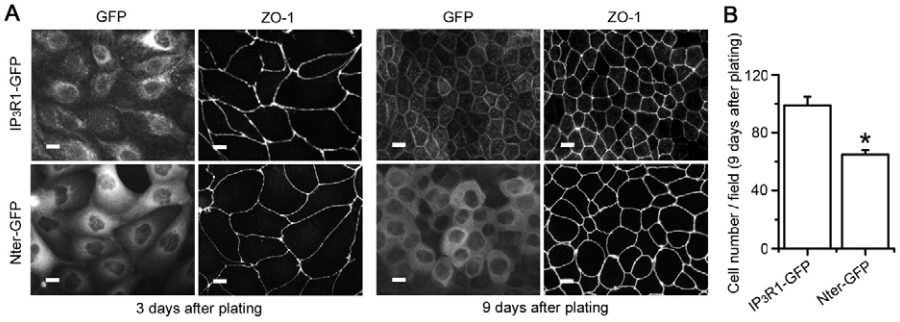

Fig. 1. Subcellular localization of Nter-GFP in subconfluent and confluent MDCK cells. (**A**) 3 days (left panels) or 9 days (right panels) after plating, MDCK cells expressing either Ins(1,4,5)P_3R1-GFP (IP$_3$R1-GFP) or Nter-GFP were fixed, permeabilized and probed with an anti ZO-1 antibody to highlight the cell-cell contact sites. The subconfluent and confluent monolayers were then stained with a secondary antibody conjugated to Alexa Fluor 548. Images were acquired with a ×63 oil-immersion objective and filter sets for FITC and Rhodamine. Scale bars: 10 μm. (**B**) Bar graphs showing that, 9 days after plating, the Nter-GFP monolayer is composed of fewer cells than the Ins(1,4,5)P_3R1-GFP monolayer. For each experiment, images were collected from ten different fields and the cell number per field was determined manually. Means ± s.e.m. of n=3 experiments; *P<0.05.

Nter-GFP expression appeared to slow down rather than accelerate the entry into the G0 phase.

To test whether the reduced cell density and the sustained expression of PCNA in Nter-GFP cells were due to an increased rate of apoptosis, cell monolayers were stained 7 days after plating with the nuclear dye Hoechst 33342 and for the ZO-1 protein. The percentage of piknotic nuclei was found to be very low (<1/1000) and not significantly different in Nter-GFP- and Ins(1,4,5)P_3R1-GFP-expressing cells, indicating that both populations were equally viable at the time of observation. By contrast, ZO-1 immunostaining revealed a higher proportion of multinucleated cells in Nter-GFP monolayers compared with control cells (3.7±0.4% versus 0.6±0.1%, n=3), suggesting an impairment of cytokinesis (Fig. 2C). This increase in the frequency of multinucleated cells was, however, too small to fully account for the lower cell density of confluent Nter-GFP monolayers.

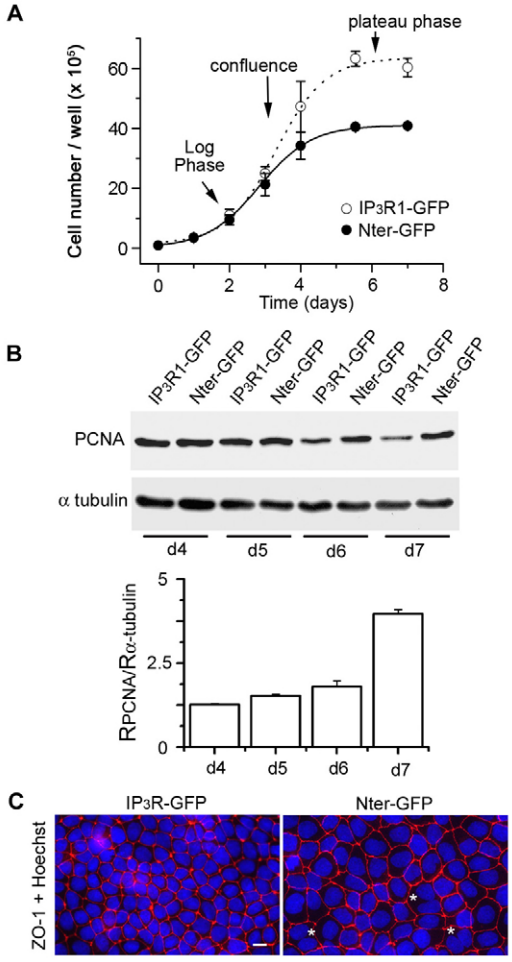

Fig. 2. Nter-GFP expression slows down the entry of confluent MDCK cells into G0 and results in an increase of multinucleated cells. (**A**) Growth curves of cells that express Ins(1,4,5)P_3R1-GFP (IP$_3$R1-GFP) or Nter-GFP. Transfected MDCK cells, seeded at time zero into six-well plates at a density of 10^5 cells/well, were trypsinized and counted using a hemocytometer at the indicated time points. Values shown are averages of the results obtained in two independent experiments ± s.d. (**B**) Ins(1,4,5)P_3R1-GFP or Nter-GFP expressing cells were lyzed every 24 hours from day (d) 4 until day 7 after plating. The extracted proteins were fractionated by SDS-PAGE and western blotting analysis was performed using either an anti-PCNA antibody or an anti-α-tubulin antibody. The upper panels show representative immunoblots. The lower panel illustrates densitometric analysis of scanned immunoblots, carried out with NIH image J software (n=3). PCNA and α-tubulin intensities derived from Nter-GFP cells were divided by the respective signals derived from Ins(1,4,5)P_3R1-GFP cells to determine R_{PCNA} and $R_{tubulin}$ values. Shown are $R_{PCNA}/R_{tubulin}$ ratios calculated at the indicated times and reflecting the increase in PCNA content of Nter-GFP cells compared with control cells. (**C**) 7 days after plating, confluent monolayers expressing Ins(1,4,5)P_3R1-GFP or Nter-GFP were stained with Hoechst 33342 to detect nuclei and for ZO-1 to visualize cell perimeters. The representative images shown were acquired with a ×40 oil-immersion objective and filter sets for DAPI and Texas red. Asterisks highlight multinucleated cells.

Nter-GFP expression results in cell-shape changes but preserves apical-basal polarity and TJ integrity

The cross-sectional area of confluent Nter-GFP cells, at steady state, was ~1.5 times larger than that of control cells, as predicted from a monolayer with reduced cell density and as evidenced by the ZO-1 immunostaining. To further evaluate the impact of Nter-GFP expression on both epithelial morphology and apical-basal polarity, confluent monolayers were immunostained for E-cadherin (a lateral marker), gp114 (an apical marker) or ZO-1, and then imaged by confocal microscopy. As shown in Fig. 3A, Nter-GFP expression resulted in reduced cell height, the loss of lateral membrane

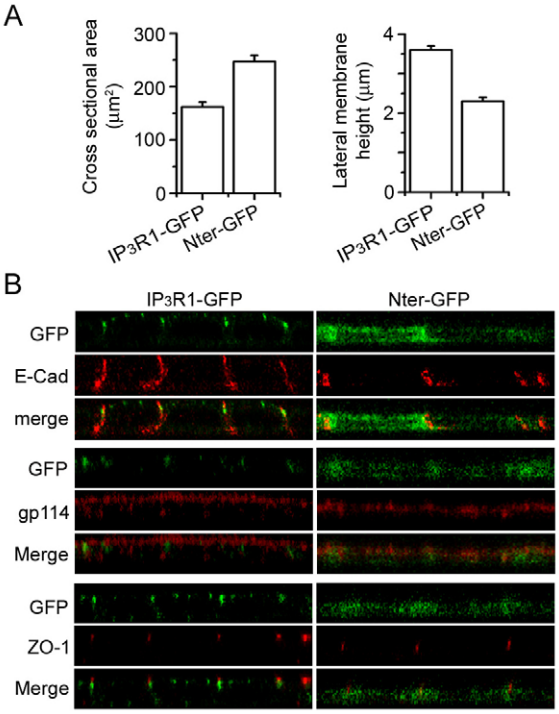

Fig. 3. Nter-GFP expression results in cell-shape changes without affecting apical-basal polarity. Plateau-phase MDCK cells expressing Ins(1,4,5)P_3R1-GFP (IP$_3$R1-GFP) or Nter-GFP were fixed, immunostained for E-cadherin, gp114 or ZO-1 and imaged by confocal microscopy. (**A**) Bar graphs showing the loss of lateral membrane height and the enlargement of apical surface area in Nter-GFP cells compared with control cells. Results are means ± s.d. of two independent experiments. For each experiment, images were collected from 10-12 different fields and analyzed with EC viewer software (Nikon). For each frame, lateral domains were manually traced and quantified and the field area was divided by the number of cells. (**B**) Representative x-z projections showing the distribution of E-cadherin (E-Cad), gp114 and ZO-1 in Ins(1,4,5)P_3R1-GFP and Nter-GFP cells. x-z distance: 7.2 μm.

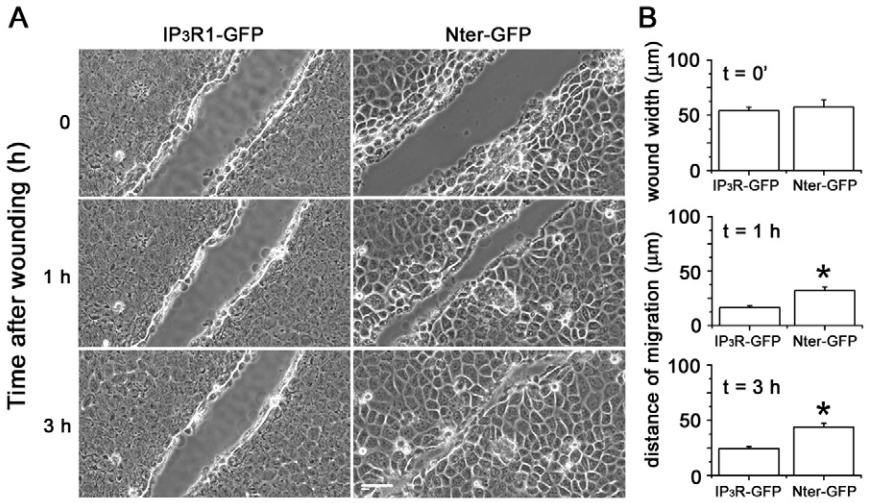

Fig. 4. Effects of Nter-GFP expression on the wound-healing ability of MDCK epithelial sheets. Polarized monolayers expressing Ins(1,4,5)P_3R1-GFP (IP_3R1-GFP) or Nter-GFP were wounded with a scalpel tip and migration of the cells into the depopulated area was evaluated by using the Nikon BioStation IM equipped with a ×40 dry objective. (**A**) Phase-contrast images of representative fields taken immediately after mechanical damage (t=0) as well as 1 hour and 3 hours later. Scale bar: 50 µm. (**B**) Bar graphs showing the wound width at t=0 and the distance covered by Nter-GFP or control cells 1 hour or 3 hours after wounding. Nine individual wounds from three independent experiments were analyzed. Data represent means ±s.e.m. (n=3, *P<0.05).

compensating for the expansion of apical and basal surfaces. The asymmetrical distribution of proteins between the apical and basolateral membrane domains was nevertheless preserved because E-cadherin was normally restricted to the lateral domain, gp114 retained its apical localization and ZO-1 was still present at the border of the apical and lateral surfaces (Fig. 3B). These results suggest that Nter-GFP expression alters epithelial cell shape but does not affect the apical-basal polarity nor drastically change the localization of representative molecules from TJs and adherens junctions.

To further investigate the ability of Nter-GFP cells to form functional TJs, transepithelial resistance (TER) measurements were performed, over 7 days (supplementary material Fig. S3). After plating, Ins(1,4,5)P_3R1-GFP cells showed a rapid increase in TER that reached 530±49 Ω.cm^2, as the cell culture became confluent. The TER development was not significantly delayed in cells expressing Nter-GFP. By contrast, the maximal value reached (996±13 Ω.cm^2) was about twice as high as that in control cells. After the peak, both cell lines recovered a similar steady state TER of 130-150 Ω.cm^2 by day 6, suggesting that junctional sealing was not dramatically impaired in Nter-GFP cells.

Polarized Nter-GFP cells display an increased mobility after wounding

A vital characteristic of epithelia is their ability for wound repair in response to injury. Wound closure involves rapid morphological changes, including cell spreading. Because Nter-GFP expression converts columnar cells into squamous cells, we inferred that the deletion mutant might modulate the dynamic processes involved in epithelial migration. To test this hypothesis, polarized monolayers expressing Ins(1,4,5)P_3R1-GFP or Nter-GFP were scratched with a scalpel tip to create a linear wound. The latter was gradually healed by cells migrating from both edges toward the center of the wound, and the distances between the opposing edges were quantified by time-lapse microscopy over a 3 hour period. As shown in Fig. 4, the velocity of Nter-GFP cells was significantly greater than that of control cells, indicating that despite their flattened morphology, Nter-GFP cells were able to migrate faster than Ins(1,4,5)P_3R1-GFP cells.

Nter-GFP associates with F-actin in subconfluent MDCK cells

A previous study has suggested a physical interaction between Ins(1,4,5)P_3Rs and the actin cytoskeleton in MDCK cells, based on the detergent insolubility of a population of Ins(1,4,5)P_3Rs (Bush et al., 1994). To explore a potential structural and functional link between F-actin and Nter-GFP, we next examined the effects of F-actin disorganization on the distribution of Nter-GFP in subconfluent cells. The latter were incubated for 1 hour with 3 µM cytochalasin D or with the drug vehicle DMSO and then stained for F-actin with Rhodamine-phalloidin (Fig. 5A). In control conditions, F-actin predominantly formed stress fibers just above the basal membrane,

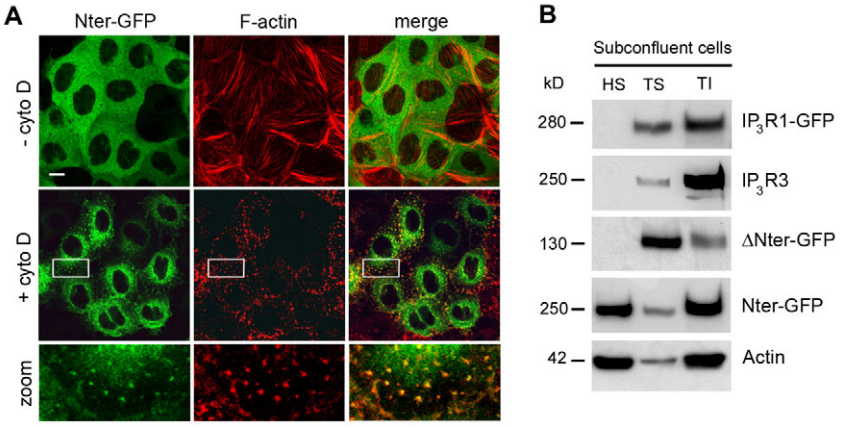

Fig. 5. Nter-GFP associates with F-actin in MDCK cells. (**A**) Fluorescence confocal images of F-actin stained with Rhodamine-phalloidin in subconfluent Nter-GFP cells treated with DMSO (upper panels) or cytochalasin D (middle panels). The lower panels represent magnified views of boxed areas. Scale bar: 10 µm. (**B**) Subconfluent or polarized MDCK cells expressing Ins(1,4,5)P_3R1-GFP (IP_3R1-GFP), ΔNter-GFP or Nter-GFP were lyzed by osmotic shock and sequentially extracted with Triton X-100 and SDS to partition cellular proteins into hydro-soluble (HS), Triton-X-100-soluble (TS) and Triton-X-100-insoluble (TI) fractions. An aliquot of each fraction (30 µg protein) was then separated by SDS-PAGE and probed with antibodies recognizing GFP, Ins(1,4,5)P_3R3 or actin. The immunoblots shown are representative of three to four independent experiments.

whereas Nter-GFP staining was diffuse throughout the cytosol. In cytochalasin-D-treated cells, the stress fibers were disrupted and reorganized into aggregates scattered into the cytoplasm; Nter-GFP was no longer evenly distributed and part of it was detected in the same spots as F-actin.

If Nter-GFP is linked to the actin cytoskeleton, it might be expected to be resistant to extraction by non-ionic detergents. To test this hypothesis, subconfluent cells expressing Nter-GFP, Ins(1,4,5)P_3R1-GFP or ΔNter-GFP were homogenized in hypotonic buffer. Three fractions – hydro-soluble (HS), Triton X-100 soluble (TS) and Triton X-100 insoluble (TI) – were then sequentially collected by centrifugation and subjected to SDS-PAGE and western blotting. As shown in Fig. 5B, the majority of Ins(1,4,5)P_3R3 and Ins(1,4,5)P_3R1-GFP molecules and about one-third of the total Nter-GFP protein were present in the actin-enriched TI fraction. By contrast, ΔNter-GFP was predominantly Triton X-100 soluble. Taken together, these results strongly suggest that Nter-GFP interacts with the actin cytoskeleton in subconfluent MDCK cells.

Nter-GFP associates with myosin IIA in both subconfluent and polarized MDCK cells

A range of cytoskeletal components have been identified that interact directly or indirectly with Ins(1,4,5)P_3Rs (Sugiyama et al., 2000; Tuvia et al., 1999; Tu et al., 1998). However, myosin II proteins more specifically aroused our interest for two reasons. First, they have been shown to associate with the N-terminal domain of ITR-1, the *Caenorhabditis elegans* Ins(1,4,5)P_3R (Walker et al., 2002). Second, myosin II proteins are known to have a fundamental role in regulating cytokinesis, cell morphology and cell migration (for reviews, see Sellers, 2000; Conti et al., 2008). Thus, we next analyzed the subcellular distribution of myosin IIA in subconfluent Nter-GFP cells treated or not with cytochalasin D. In control conditions, myosin IIA accumulated strongly at stress fibers (Fig. 6A, upper panels). By contrast, in cytochalasin-D-treated cells, myosin IIA labeling became concentrated in very bright foci that are scattered throughout the cytosol and look similar to the F-actin aggregates observed previously. Again, several of these foci, which probably represent contracted stress fibers, were co-stained by Nter-GFP (Fig. 6A, lower panels).

To determine whether Nter-GFP physically interacts with myosin IIA, whole-cell lysates prepared from subconfluent or polarized Nter-GFP cells were subjected to co-immunoprecipitation with either anti-GFP antibodies or normal rabbit IgG. The input and immunoprecipitated proteins were then separated by SDS-PAGE and probed with anti-GFP or anti-myosin-IIA antibodies. As shown in Fig. 6B (upper panels), regardless the differentiation state of the cells, a small amount of myosin IIa (when compared with the input material) was co-immunoprecipitated by anti-GFP antibodies, but not (or barely) by control IgGs. These observations suggest that Nter-GFP interacts with a small pool of myosin IIA in both subconfluent and polarized MDCK cells. When similar experiments were performed with Ins(1,4,5)P_3R1-GFP expressing cells, myosin IIA was found to significantly and reproducibly associate with Ins(1,4,5)P_3R1-GFP only in polarized cells (Fig. 6B, lower panels).

Nter-GFP expression impairs the formation of the perijunctional myosin ring in polarized MDCK cells

These results led us to compare the subcellular localization of myosin IIA in polarized cells expressing either Ins(1,4,5)P_3R1-GFP or Nter-GFP. Images of *x-y* confocal sections performed across the Ins(1,4,5)P_3R1-GFP cell monolayer revealed that myosin IIA immunostaining differed depending on the focal plane position along the apicobasal axis (Fig. 7A). Just above basal membranes, myosin IIA strongly accumulated at stress fibers. At the middle level, the actin-based motor was distributed almost evenly throughout the cytoplasm (not shown). At the cell apex, myosin IIA predominantly assembled into a ring circumscribing the cell (Fig. 7A) and co-localized with the TJ protein ZO-1 (Fig. 7B,C). Association of myosin IIA with stress fibers was rather preserved in Nter-GFP cells. By contrast, at the apical level, the motor protein no longer formed a continuous belt, but appeared as small filaments scattered throughout the cytoplasm (Fig. 7A). Concomitantly, the relative pixel intensity of myosin IIA fluorescence at the TJ level was significantly decreased in Nter-GFP cells compared with control cells (Fig. 7B,C).

To better characterize the perijunctional ring of myosin IIA detected in control cells, polarized MDCK cells expressing Ins(1,4,5)P_3R1-GFP were co-stained for F-actin and myosin IIA. As shown in supplementary material Fig. S4A, the myosin ring was also intensely labeled with Rhodamine-phalloidin, suggesting that it corresponds to the well-characterized actomyosin contractile belt associated with the apical junctional complex.

To determine whether Nter-GFP expression was accompanied by F-actin reorganization at the TJ level, polarized monolayers expressing Nter-GFP or Ins(1,4,5)P_3R1-GFP cells were doubly stained with an anti-Claudin-2 antibody and Rhodamine-phalloidin.

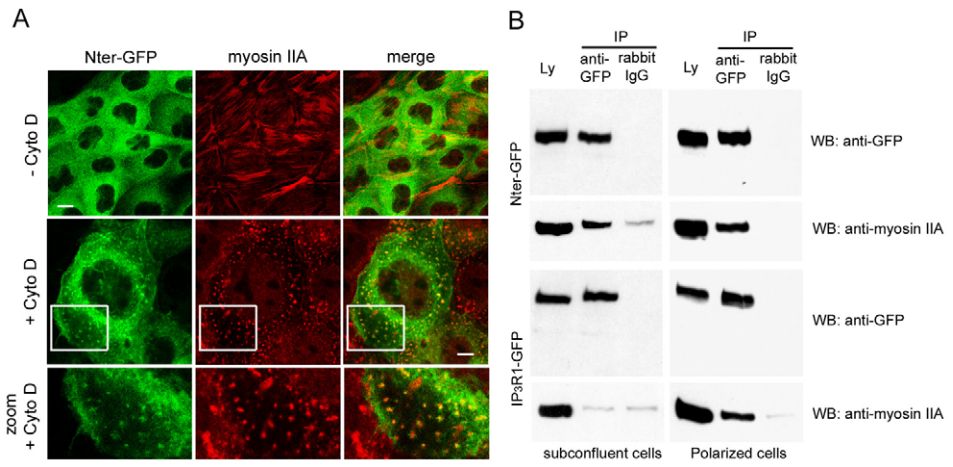

Fig. 6. Nter-GFP is linked to myosin IIA in both proliferating and polarized cells. (**A**) MDCK cells treated with DMSO (upper panels) or cytochalasin D (middle and lower panels) were fixed, permeabilized, stained for myosin IIA and analyzed by confocal microscopy. The lower panels represent magnified views of boxed areas. Scale bars: 10 μm (upper panels), 2.5 μm (middle panels). (**B**) Total cell lysates prepared from subconfluent or polarized MDCK cells expressing either Ins(1,4,5)P_3R1-GFP (IP$_3$R1-GFP) or Nter-GFP were immunoprecipitated with anti-GFP or normal rabbit antibodies. Samples were fractionated by SDS-PAGE and blotted for GFP or myosin IIA. The immunoblots shown are representative of two independent experiments. Ly: total cell lysate; IP: immunoprecipitation; WB: western blot.

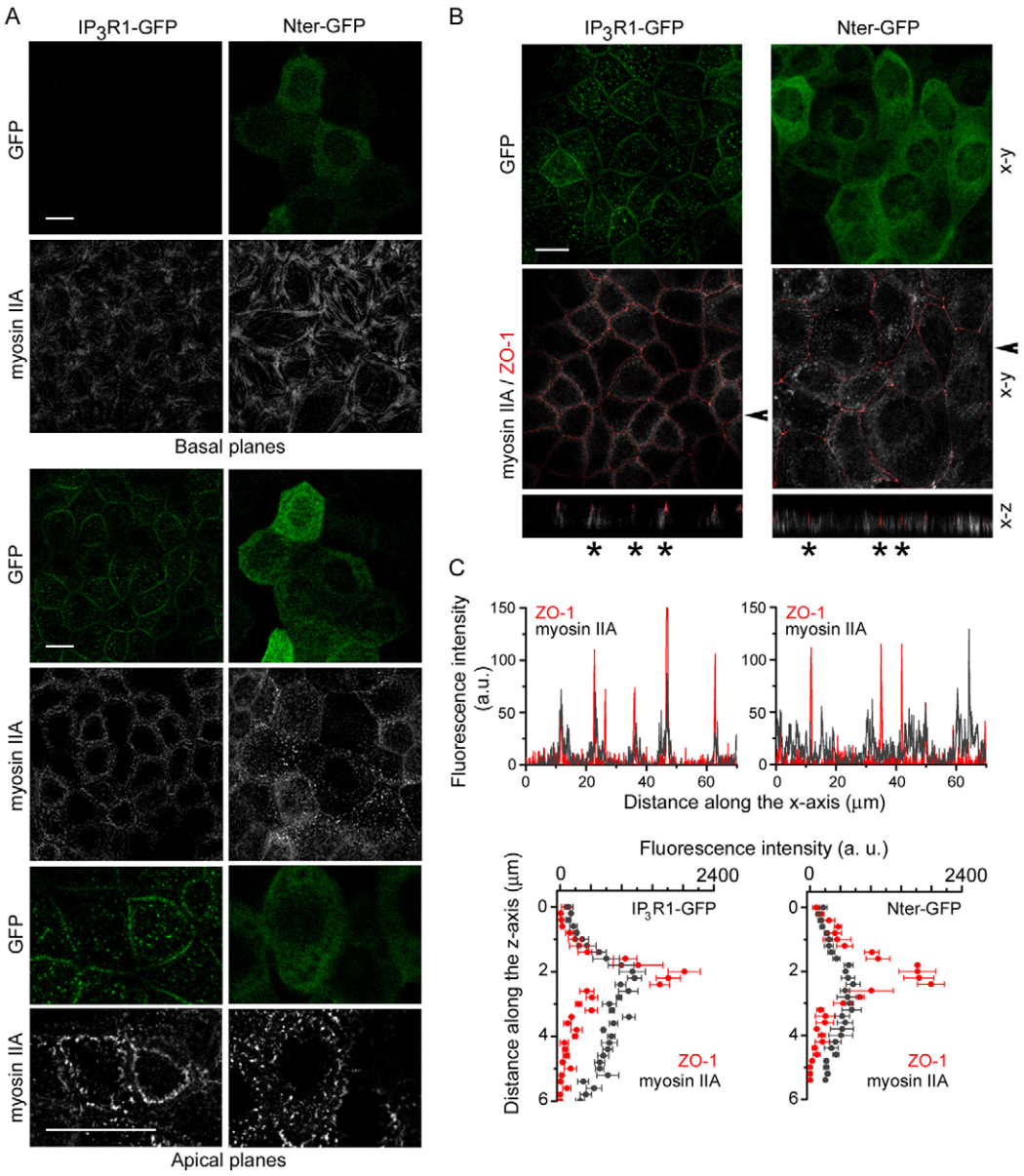

Fig. 7. Nter-GFP expression prevents the formation of the subapical myosin ring in polarized MDCK cells. (**A**) Polarized MDCK cells expressing Ins(1,4,5)P_3R1-GFP (IP$_3$R1-GFP) or Nter-GFP were fixed, permeabilized and immunostained for myosin IIA. Single confocal sections captured at the basal planes and apical planes are shown. Scale bars: 10 μm. (**B**,**C**) Polarized Ins(1,4,5)P_3R1-GFP- or Nter-GFP-expressing cells were fixed, permeabilized and double labeled with a mixture of antibodies against myosin IIA and ZO-1. Confocal images were then acquired in the same conditions and identically processed for quantitative analysis. Individual *x*-*y* sections captured at the TJ level (as defined by ZO-1 immunostaining) and *x*-*z* projected views are presented in B. Intensity profiles of myosin IIA and ZO-1 fluorescence (means ± s.d.) obtained along the *x*-axis at the TJ level (upper panels) or along the *z*-axis (lower panels) are shown in C. Arrowheads denote positions of the *x*-*z* projections. Asterisks highlight the cell-cell contact sites along which the pixel intensities of myosin IIA or ZO-1 fluorescence were quantified and averaged at each optical section. The results shown are representative of two independent experiments. a.u., arbitrary units. Scale bar: 10 μm; *x*-*z* distance: 7.2 μm.

As shown in supplementary material Fig. S4B, continuous belts of F-actin anchored to TJs were observed in the apical region of both control and Nter-GFP cells. However, although the actin belts of adjacent cells could be easily distinguished from each other in Ins(1,4,5)P_3R1-GFP cells, they rather appeared as single lines at cell-cell borders in Nter-GFP cells. This observation is consistent with the results depicted above, because it might indicate that the centripetal contractile force normally imposed by myosin IIA on the perijunctional actin belts is decreased in Nter-GFP cells (supplementary material Fig. S4C).

Nter-GFP expression reduces accumulation of endogenous Ins(1,4,5)P_3R3 at the apex of the lateral membrane

If myosin IIA is required for the recruitment of Ins(1,4,5)P_3Rs near the tight junctions, Nter-GFP expression might be expected to also affect the subcellular localization of endogenous Ins(1,4,5)P_3R3 in polarized cells. As shown in Fig. 8A, Nter-GFP expression did not fully prevent the translocation of Ins(1,4,5)P_3R3 to the cell periphery upon epithelial cell differentiation. However, quantification of the relative pixel intensities of claudin-2 and Ins(1,4,5)P_3R3

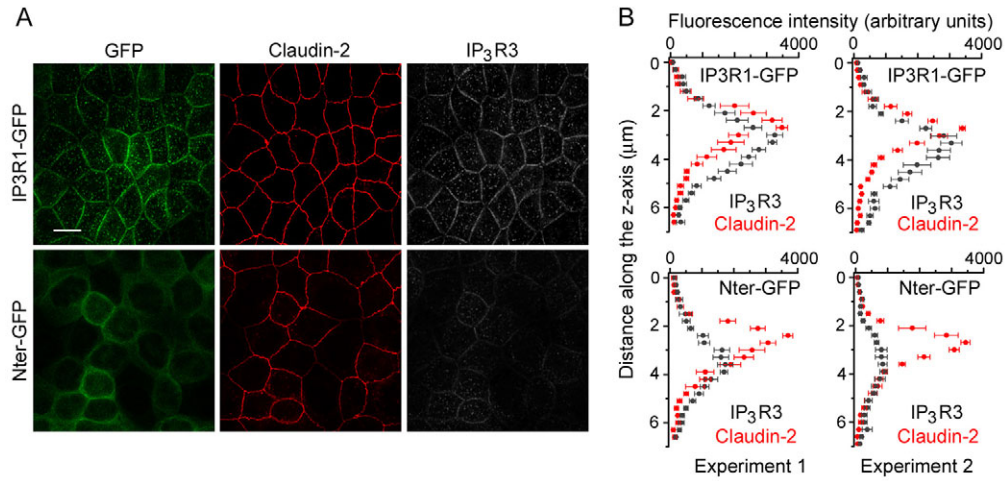

Fig. 8. Nter-GFP expression affects Ins(1,4,5)P_3R3 accumulation near the TJ in polarized MDCK monolayers. Polarized MDCK cells expressing Ins(1,4,5)P_3R1-GFP (IP$_3$R1-GFP) or Nter-GFP were fixed, co-stained for Ins(1,4,5)P_3R3 and claudin-2 and then imaged by confocal microscopy. (**A**) Representative images showing the distribution of either Ins(1,4,5)P_3R1-GFP or Nter-GFP (green), claudin-2 (red) and Ins(1,4,5)P_3R3 (gray) in single confocal *x-y* sections. Scale bar: 10 µm. (**B**) Relative pixel intensities of claudin-2 and Ins(1,4,5)P_3R3 fluorescence along cell-cell junctions. For each experiment, and for each cell line, six cell-cell junctions were randomly selected in two independent fields scanned under the same conditions and the relative pixel intensities of claudin-2 and Ins(1,4,5)P_3R3 fluorescence along these junctions were determined using the EC viewer software (pixel size, 70 nm; *z* step, 0.3 µm). The results shown are averaged values at each optical section ± s.e.m. for two independent experiments.

fluorescence at each optical section revealed that, in polarized Nter-GFP cells, Ins(1,4,5)P_3R3 accumulation in the immediate vicinity of the TJ marker claudin-2 was significantly reduced (Fig. 8B).

Knockdown of myosin IIA expression in confluent MDCK cells mimics the effects of Nter-GFP expression on epithelial cell shape

To further investigate whether myosin IIA has a role in Ins(1,4,5)P_3R3 localization in polarized MDCK cells, we tried to downregulate myosin IIA expression in wild-type MDCK cells by RNA interference. Cells were transfected just after they had reached confluence with either siRNA against canine myosin IIA or with a nonsense duplex. Under those experimental conditions, the immunofluorescence signal obtained after incubation with the anti-myosin-IIA antibody followed by a secondary antibody coupled to Alexa Fluor 488 was substantially reduced in 10-15% of the cells treated with the myosin-IIA-targeted siRNAs (Fig. 9A). Such a reduction was not observed when the primary antibody was directed against myosin IIB (supplementary material Fig. S5) or when MDCK cells were transfected with the nonsense siRNA (Fig. 9A).

In assessing the effects of myosin IIA knockdown on polarized MDCK cells, we first noticed alterations in cell morphology. As evidenced by ZO-1 immunostaining, myosin-IIA-depleted cells showed increased apical area (Fig. 9B) and decreased lateral height (Fig. 9C) when compared with neighboring cells that were positive for myosin IIA, or with cells treated with nonsense siRNA. These changes in shape, which were reminiscent of those induced by Nter-GFP expression, were observed with both the myosin-IIA-targeted siRNAs tested.

The distribution of Ins(1,4,5)P_3R3 along the lateral membrane domain was then compared with that of ZO-1 in myosin-IIA-positive and myosin-IIA-depleted cells from the same monolayer. As shown in Fig. 10A, Ins(1,4,5)P_3R3 was still discernible at the periphery of myosin-IIA-depleted cells (white arrows). However, quantification of the relative pixel intensities of ZO-1 and Ins(1,4,5)P_3R3 fluorescence in each *x-y* optical section revealed that, whereas myosin-IIA-positive cells normally accumulated Ins(1,4,5)P_3R3 at the apex of the lateral membrane (Fig. 10B, positions 2 and 4), myosin-IIA-depleted cells did not (Fig. 10B, positions 1 and 3). These changes in Ins(1,4,5)P_3R3 distribution were again very similar to those observed in Nter-GFP-expressing cells and could be reproduced with the two myosin-IIA-targeted siRNAs tested (not shown). Taken together, these results suggest that myosin IIA is required for the recruitment of Ins(1,4,5)P_3R3 at the apex of the lateral domain in polarized MDCK cells and that the phenotypic changes associated with Nter-GFP expression are probably caused by a partial impairment of myosin IIA function, leading to a decrease in cortical tension.

Discussion

Ins(1,4,5)P_3R isoforms are often distributed heterogeneously within cells and in patterns that differ between cell types. Although it is clear that spatial restriction of Ca^{2+} signaling is one of the mechanisms used by the cells to ensure the appropriate response to a given stimulus, very little is known about the molecular mechanisms that regulate Ins(1,4,5)P_3R localization. In the present study, we propose that myosin IIA has a crucial function in recruiting Ins(1,4,5)P_3Rs in the vicinity of tight junctions in MDCK epithelial cells. This conclusion is based on the complementary results of several experimental approaches.

Co-immunoprecipitation studies revealed that the N-terminal domain of Ins(1,4,5)P_3R1-GFP which is required for the accumulation of the Ca^{2+} channel at the TJ level, associates with myosin IIA when stably expressed in MDCK cells. Full-length Ins(1,4,5)P_3R1-GFP was also found to bind myosin IIA in polarized MDCK cells suggesting that the interaction with the actin-based motor was not just the consequence of removing the ER membrane anchor. This observation is consistent with a previous study indicating that the N-terminal domain of ITR-1, the *C. elegans* Ins(1,4,5)P_3R, directly binds to the C-terminal region of myosin II

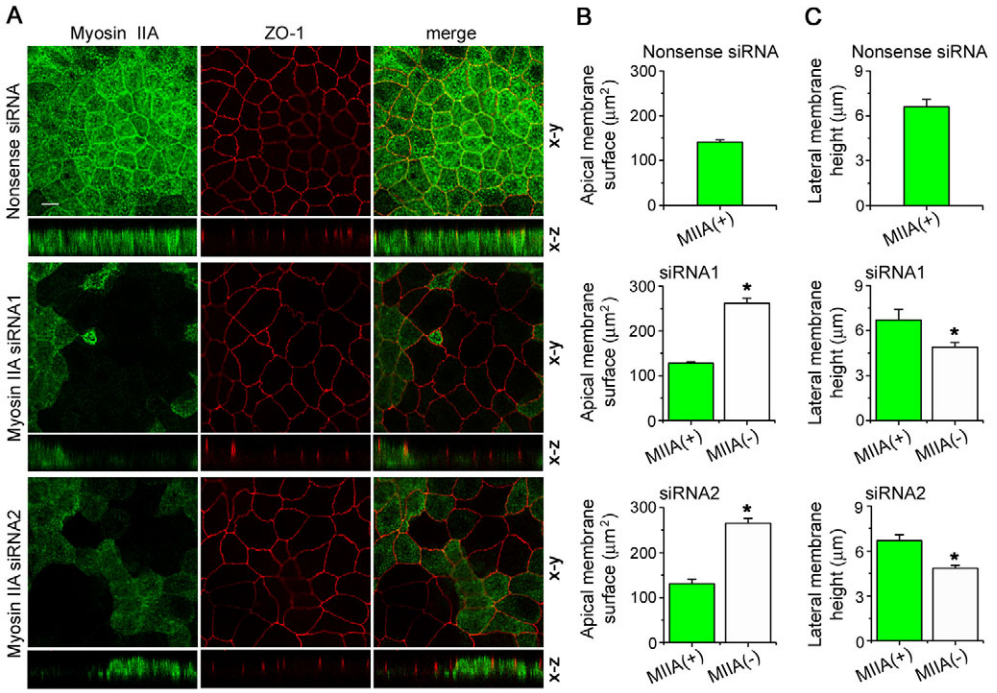

Fig. 9. Downregulation of myosin IIA expression by RNA interference alters wild-type MDCK cell morphology. Confluent MDCK cells were transfected with either nonsense or myosin IIA-targeted siRNAs and on day 3 after transfection, were fixed and stained for myosin IIA and ZO-1. (**A**) Representative confocal *x-y* and *x-z* sections showing myosin IIA (green) and ZO-1 (red) distribution in the siRNA-treated cells. Scale bar: 10 μm; *x-z* distance: 8.4 μm. (**B**) Bar graphs showing the enlargement of apical surface area (delimited by ZO-1 staining) in myosin-IIA-depleted cells. Results are means ± s.e.m. of three independent experiments. For each experiment, images were collected from 6-7 independent fields and analyzed with NIH imageJ software. (**C**) Bar graphs showing the loss of lateral membrane in myosin IIA-depleted cells. The distance separating the ZO-1 signal from the basal surface of the cells was measured, using the EC viewer software (Nikon), in myosin-IIA-positive or myosin-IIA-depleted cells. Five to six independently scanned fields were analyzed and the results shown are means ± s.e.m. MIIA(-), myosin IIA-depleted cells; MIIA(+), nonsense siRNA-treated cells (upper panels) or myosin-IIA-positive cells present in the same field as the knockdown cells (middle and lower panels).

heavy chains from both muscle and non-muscle origin (Walker et al., 2002), and that the interacting regions are highly conserved between invertebrates and mammals.

Nter-GFP expression was found to specifically affect the perijunctional localization of myosin IIA in polarized MDCK cells. The underlying mechanism remains elusive, but is probably not related to inhibition of myosin IIA polymerization because myosin filaments were still assembled and normally incorporated into basal stress fibers in Nter-GFP cells. Interestingly, a recent study has identified in the tail domain of zipper, the *Drosophila* non-muscle myosin II heavy chain, a region that is required for its recruitment to the cell periphery and is almost entirely distinct from the filament-assembly domain (Liu et al., 2008). This sequence, containing residues 1350 to 1865 is well conserved in canine myosin IIA and includes the region of the non-muscle myosin II heavy chain NMY-2, which is known to interact with ITR-1 in *C. elegans* (Walker et al., 2002). Thus, one possibility is that Nter-GFP alters myosin IIA localization by preventing access to the cortical-targeting domain of the motor protein. Alternatively, Nter-GFP might interfere with anchorage of myosin IIA at TJs, through the protein cingulin, because the N-terminal domain of ITR-1 (Walker et al., 2002) and cingulin (Cordenonsi et al., 1999) have both been reported to bind to the C-terminal coiled-coil region of myosin II.

Nter-GFP expression induced numerous phenotypic changes that all suggest a decrease in cortical tension and are therefore consistent with an impaired localization of myosin IIA to the perijunctional actin belt. In the first place, the contractile forces generated by myosin II at the cell periphery have been shown to control the cell-shape changes that occur during epithelial morphogenesis and also the cell-packing geometry at steady state (Farhadifar et al., 2007; Ivanov et al., 2007). Thus, mistargeting of myosin IIA to the perijunctional actin ring is likely to prevent the apical constriction required for cell compaction during monolayer formation and might explain the increase in the cross-sectional area observed in Nter-GFP cells. The concomitant reduction of cell height could then be interpreted as a strategy to keep the cell volume constant and the reduced cell density at confluence as a consequence of the flattened morphology. This hypothesis is further supported by the fact that other processes known to influence steady-state cell density (including premature exit from the cell cycle, cell growth inhibition or increased rate of apoptosis) did not appear to affect Nter-GFP cells. In addition, the contractile forces generated by non-muscle myosin II are believed to regulate cytokinesis in animal cells (Glotzer, 2000; Robinson and Spudich, 2004; Bao et al., 2005) and cytokinesis failure was observed more frequently in confluent monolayers expressing Nter-GFP than in those expressing Ins(1,4,5)P_3R1-GFP. By contrast, subconfluent Nter-GFP cells appeared to divide as efficiently as control cells, suggesting that myosin IIA is dispensable for cytokinesis as long as the two daughter cells can move away from one another. This is reminiscent of the previously reported behavior of normal rat kidney fibroblasts treated with blebbistatin, a potent myosin II inhibitor (Kanada et

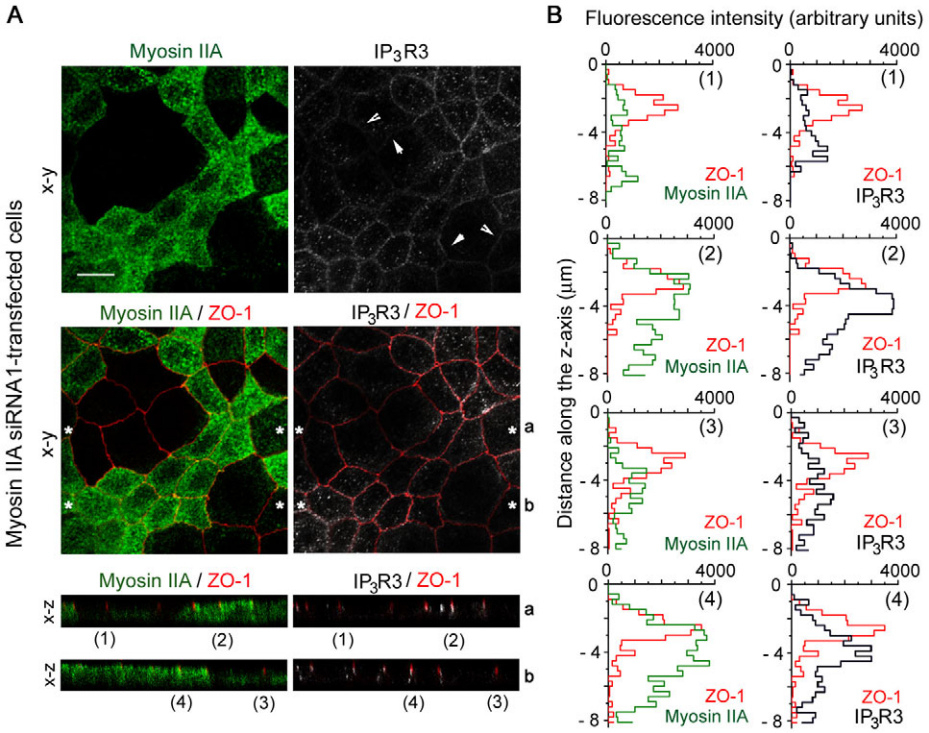

Fig. 10. Effects of myosin IIA suppression by siRNA on accumulation of Ins(1,4,5)P_3R3 at the apex of the lateral membrane. Confluent MDCK cells were transfected with the myosin-IIA-targeted siRNA1 and on day 3 after transfection, were fixed and simultaneously immunostained with a mixture of antibodies against myosin IIA, Ins(1,4,5)P_3R3 and ZO-1. (**A**) Representative confocal *x-y* sections and *x-z* projections showing the localization of myosin IIA (green), ZO-1 (red) and Ins(1,4,5)P_3R3 (gray) in the siRNA-treated cells, as single colour images (upper panels) or two-colour merged images (middle and lower panels). Scale bar: 10 µm; *x-z* distance: 8.4 µm. (**B**) Relative pixel intensities of ZO-1, Ins(1,4,5)P_3R3 and myosin IIA fluorescence at each optical section, from the apex to the basal surface of the cell. (1) and (3): cell-cell junctions between myosin IIA-depleted cells; (2) and (4): cell-cell junctions between myosin-IIA-positive cells. Arrows indicate cortically positioned Ins(1,4,5)P_3R3 in myosin-IIA-depleted cells. a and b represent two different *x-z* views and asterisks indicate the position at which they were generated.

al., 2005). The latter, when grown on fibronectin-coated surfaces, were able to undergo cytokinesis by making use of polar traction forces, and the blebbistatin-resistant cytokinesis pathway was impaired only if the advance of the lamellipodia emitted by the mitotic cells was prevented by neighboring cells. Finally, Nter-GFP cells exhibited increased motility after monolayer wounding, as previously reported for myosin-IIA-ablated embryonic stem cells or for breast epithelial cells and fibroblasts treated with blebbistatin (Even-Ram et al., 2007; Shutova et al., 2008). This result is in agreement with previous reports suggesting on the one hand that the closure of large linear wounds occurs by the process of Rac- and phosphoinositide-dependent cell crawling and not by purse-string contraction of the perijunctional actomyosin belt (Nobes and Hall, 1999; Fenteany et al., 2000), and, on the other hand, that cortical myosin activity is not required for large-wound re-epithelialization and can even antagonize cell migration (Even-Ram et al., 2007).

Suppression of myosin IIA expression in wild-type MDCK cells with siRNAs further supported the hypothesis that Nter-GFP acts through partial impairment of myosin IIA organization and function. Although transfection efficiency appeared to be very low in our experimental conditions (probably because siRNAs were applied to confluent monolayers), myosin-IIA-depleted cells could be unambiguously identified by immunofluorescence and were found to exhibit the same morphological alterations as seen in Nter-GFP-expressing cells, as well as mild defects in cytokinesis (not shown). Furthermore, myosin IIA depletion by RNA interference, similarly to Nter-GFP expression, was shown to reduce the accumulation of Ins(1,4,5)P_3R3 at the TJ level in polarized MDCK cells, strongly suggesting that myosin IIA is required for the recruitment and/or the sequestration of Ins(1,4,5)P_3Rs at the TJ level.

The question that arises now is whether functional significance can be assigned to Ins(1,4,5)P_3R-myosin-II complexes in MDCK cells. In *C. elegans*, the interaction between ITR-1 and myosin II was demonstrated to be necessary for the upregulation of pharyngeal pumping in response to food (Walker et al., 2002) and Ins(1,4,5)P_3Rs are also thought to regulate myosin-II-driven contraction in a large number of mammalian cell types, including epithelial cells. In hepatocytes, for example, both type 2 Ins(1,4,5)P_3Rs and myosin II are enriched in the pericanalicular region and myosin-driven contraction of bile canaliculi follows and requires Ins(1,4,5)P_3-dependent Ca^{2+} release (Dufour et al., 1995; Hirata et al., 2002). The prevailing idea is that Ins(1,4,5)P_3R-operated Ca^{2+} release leads to phosphorylation of the myosin light chain (MLC) by the Ca^{2+}/calmodulin-dependent MLC kinase (MLCK), thereby increasing myosin II ATPase activity and filament formation. In MDCK cells, MLCK activation induces purse-string contraction of the perijunctional actomyosin belt (Hecht et al., 1996), but does not seem to be essential for central stress-fiber assembly and dynamics (Sutton et al., 2001). Thus, as previously shown for cultured human fibroblasts (Totsukawa et al., 2000), MLCK activity is probably subjected to spatial regulation in polarized MDCK cells, and compartimentalization of Ins(1,4,5)P_3Rs in the vicinity of tight junctions, through its interaction with myosin IIA, could contribute to this process. Future studies are required to confirm this hypothesis.

Materials and Methods

Materials

Dulbecco's modified Eagle's medium, fetal calf serum, penicillin/streptomycin, trypsin, Geneticin and the acetoxymethyl ester form of Fura-2 (Fura-2/AM) were purchased from Invitrogen. MDCK cells were from the American Type Culture Collection (Rockville, MD). Restriction endonucleases were purchased from Promega and Protein-G-agarose was from Roche Applied Science. All other chemicals were of the highest grade available and were obtained from Sigma.

Primary antibodies

Mouse monoclonal antibodies raised against E-cadherin and Ins(1,4,5)P_3R3 were purchased from BD Biosciences. Polyclonal antibodies against actin, myosin IIA and myosin IIB were from Sigma. Mouse monoclonal antibodies against GFP, the protein disulfide isomerase (PDI) and the proliferating cell nuclear antigen (PCNA) were from Roche Applied Science, Zymed Laboratories and Santa Cruz Biotechnology, respectively. Polyclonal antibody against claudin-2 was purchased from Zymed Laboratories. Rat monoclonal anti-ZO-1 antibody and rabbit polyclonal anti-gp114

antibody were kind gifts from Bruce Stevenson (University of Alberta, Edmonton, Canada) and André Le Bivic (Université de la Méditerannée, Marseille, France). Secondary antibodies conjugated to Alexa Fluor 488, 546, 568 or 633 were obtained from Invitrogen.

DNA constructs

The construction of the expression plasmid encoding the mouse type 1 Ins(1,4,5)P_3R fused to the N-terminus of GFP (and referred to as pIns(1,4,5)P_3R1-GFP) has been previously described (Colosetti et al., 2003). The plasmid encoding the ΔNter-GFP mutant missing amino acids 79-1959 was obtained by ligation of the 2.4 kb *Eco*47III-*Age*I and the 5.3 kb *Sma*I-*Age*I restriction fragments excised from pIns(1,4,5)P_3R1-GFP. The construct encoding the N-terminal domain (residues 1-2217) of the mouse type 1 Ins(1,4,5)P_3R attached, via a 16 amino acid linker at its C-terminus, to EGFP (and referred as Nter-GFP) was generated as follows: pIns(1,4,5)P_3R1-GFP was digested with *Sac*I or *Bst*EII plus *Eco*RI. The 2.1 kb *Sac*I fragment and the 6.75 kb *Bst*EII-*Eco*RI fragment were gel purified and successively subcloned into pEGFP-N2 (Clontech). The sequences and junctions of all constructs were verified by restriction analysis and sequencing.

Cell culture and transfection of MDCK cells

Madin-Darby canine kidney (MDCK) cells were cultured in DMEM supplemented with 5% FCS, 100 U/ml penicillin, 100 μg/ml streptomycin sulfate and 0.25 μg/ml fungizone at 37°C in a humidity-controlled incubator with 7% CO_2. Cells were transfected by the calcium phosphate coprecipitation method. Briefly, MDCK cells were seeded onto six-well culture dishes at a density of 10^5 cells/well. 24 hours after plating, purified plasmids (5 μg) were mixed with equal volumes of 0.25 M $CaCl_2$ and 2× HEPES-buffered saline (50 mM HEPES, pH 7.1, 280 mM NaCl, 1.5 mM Na_2HPO_4). The mixture was incubated at room temperature for 30 minutes and then added dropwise to the plates. Cells were washed twice with Ca^{2+}/Mg^{2+}-free phosphate-buffered saline (PBS) 16 hours later and placed in fresh growth medium containing 600 μg/ml active G418. 3 weeks after transfection, G418-resistant cells were harvested by trypsinization and those exhibiting a marked green fluorescence were selected by FACS (FACS Vantage, Becton Dickinson) and expanded.

Immunofluorescence

Cells, attached to glass coverslips, were rinsed twice with PBS pH 7.4. Cells were either fixed at room temperature with 4% paraformaldehyde in PBS for 20 minutes and then permeabilized using 0.5% Triton X-100 in PBS for 3 minutes or first incubated for 2 minutes at 4°C with 2% formaldehyde in PBS (to prevent cell shrinkage) and then fixed/permeabilized in ice-cold methanol for 10 minutes. Blockade of nonspecific binding sites was performed by incubating the monolayers with PBS containing 0.2% gelatin for 30 minutes. Fixed cells were stained for 1 hour with the primary antibody, washed three times with the blocking solution and then incubated for 1 hour with a 1:300 dilution of the appropriate secondary antibody. All antibody dilutions were prepared in PBS supplemented with 0.2% gelatin and incubations were carried out at room temperature. After extensive washing with PBS, coverslips were mounted using Prolong antifade reagent (Molecular Probes) and viewed with an Axioskop fluorescence microscope (Zeiss, Germany) equipped with a 100 W Xe arc lamp and with standard FITC and Rhodamine filter sets. Images were collected through a ×63 or a ×40 oil-immersion objective with a CCD camera (Nikon DXm 1200) and digitized with the Act-1 imaging software (Nikon). Alternatively, cells were examined with a confocal microscope (Eclipse TE-2000-Nikon-C1, France) equipped with a ×63 plan-apochromatic oil-immersion objective (NA 1.4) and an air-cooled Argon and He-Ne lasers. Optical sections were collected at 0.3 μm intervals and images were processed using Photoshop 7 (Adobe) software.

Wound migration studies

Highly confluent MDCK cells on glass coverslips were wounded with a scalpel tip. Long scratches were made before rinsing the monolayer with fresh culture medium to remove detached cells. Fluorescence and phase-contrast images were generated by using the Nikon BioStation IM equipped with a ×40 0.8 NA plan fluor objective and captured using a cooled CCD camera. Cells, in the incubation chamber, were maintained at 37°C and with 7% CO_2. For each coverslip, three separate fields were imaged, every 2 seconds. The mean distance migrated along the wound edge was determined using Adobe Photoshop 7.0.

Preparation of membrane fractions

MDCK cells were washed twice with PBS at 4°C and then harvested in ice-cold hypo-osmotic buffer containing: 50 mM Tris-HCl, pH 7.4, 10 mM KCl, 2 mM EDTA and complete protease inhibitors (Roche). The cell lysate was subjected to three freeze-thaw cycles and then passed ten times through a 21-gauge needle to shear DNA. Normal osmolarity was restored by adding 150 mM NaCl. Cell lysates were centrifuged for 1 hour at 100,000 ***g*** and 4°C in a SW65 rotor (Beckman Coulter), resulting in a clear hydrosoluble fraction and a pellet. The latter was resuspended in ice-cold PBS supplemented with 1% Triton X-100, 2 mM EDTA and the aforementioned protease inhibitors, homogenized by ten passages through a 23-gauge needle and gently agitated on a rotating wheel at 4°C for 30 minutes. The Triton-X-100-insoluble material was collected by centrifugation at 100,000 ***g*** for 1 hour at 4°C and then solubilized in ice-cold PBS containing 1% SDS, 2 mM EDTA and protease inhibitors. Protein concentrations were determined with the bicinchoninic acid procedure using bovine serum albumin as standard. Regardless of the confluence state of the cells, proteins were distributed between the three fractions approximately as follows: hydro-soluble (HS), 70%; Triton X-100 soluble (TS), 10%; Triton X-100 insoluble (TI), 20%. Polyacrylamide gels were loaded with equal amounts of proteins (30 μg) rather than equal volumes of the three fractions.

Immunoprecipitation of the GFP-tagged constructs

Non-confluent or polarized MDCK cells were rinsed twice with ice-cold PBS pH 7.4 and then harvested in a buffer consisting of 50 mM Tris-HCl, pH 7.4, 300 mM NaCl, 2 mM EDTA, 1% Triton X-100 and complete protease inhibitors. After removal of cellular debris by centrifugation for 10 minutes at 700 ***g*** and 4°C, the MDCK cell extracts (300 μg protein per 500 μl) were preincubated with Protein-G-Sepharose beads (Amersham) by rotating for 2 hours at 4°C. The precleared lysates were then incubated with 3 μg anti-GFP antibody or normal rabbit IgG and rotated overnight at 4°C. Antigen-antibody complexes were then precipitated by adding 50 μl Protein-G-Sepharose beads pre-equilibrated in the lysis buffer supplemented with 0.5% BSA. After rocking the reaction mixtures for 2 hours at 4°C, the beads were recovered by centrifugation at 500 ***g*** for 2 minutes and washed twice with a high ionic strength buffer (containing 50 mM Tris-HCl, pH 7.4, 600 mM NaCl, 2 mM EDTA, 1% Triton X-100 and complete protease inhibitors) and twice with the lysis buffer. The immunoprecipitates were eluted by boiling the samples in 100 μl 2× Laemmli buffer for 5 minutes and then fractionated by SDS-PAGE.

SDS-PAGE and immunoblotting

Proteins were fractionated on an SDS-PAGE polyacrylamide gel and electrophoretically transferred to Immobilon-P membranes (Millipore Corp.) in 25 mM Tris-HCl, 0.19 M glycine and 20% ethanol. The polyvinylidene difluoride membranes were blocked overnight at 4°C in PBS containing 5% non-fat dry milk and 0.05% Tween 20, rinsed twice with water and then incubated for 2 hours at room temperature with the primary antibody in PBS supplemented with 0.05% Tween 20. After three washes with PBS, 0.05% Tween 20, the membrane was allowed to react for 1 hour at room temperature with a peroxidase-conjugated goat anti-rabbit or anti-mouse IgG (Amersham) as required, diluted 1:4000 in PBS, 0.05% Tween 20. The blots were washed three times with PBS, 0.05% Tween 20 and the immune complexes were visualized by chemiluminescence (ECL Western blotting analysis system, Amersham).

RNA interference

The siRNA1 (5′-CCGAAGAGAUCGUGGAAAUTT-3′) and siRNA2 (5′-GGCCAAAGCUGCCGAGUAATT-3′) duplexes targeted to canine myosin IIA were chemically synthesized by Eurogentec. Mock nontargeting control siRNA was obtained from the same purchaser. MDCK cells were plated at 10^4 cells per well in 24-well plates containing glass coverslips. Transfections were carried out after confluence was reached using the Lipofectamine RNAimax reagent (Invitrogen) in optiMEM medium (Invitrogen) and without antibiotics, according to manufacturer's protocol. The final siRNA concentration was 50 nM and 1 μl Lipofectamine RNAimax reagent was added per well. The culture medium was changed 48 hours after transfection, and cells were used for experiments 24-30 hours later.

Statistics

Data are represented as means ± s.e.m. (except where otherwise noted). Statistical comparisons were made by using the Student's unpaired *t*-test and $P<0.05$ were taken as significant. *n* represent the number of independent experiments.

We thank Oliver Nüsse and Jordi Molgó for critical reading of this manuscript. This study was supported by the University Paris South and the National Institute for Health and Medical Research (INSERM).

Supplementary material available online at
http://jcs.biologists.org/cgi/content/full/123/9/1449/DC1

References

Ashby, M. C. and Tepikin, A. V. (2002). Polarized calcium and calmodulin signaling in secretory epithelia. *Physiol. Rev.* **82**, 701-734.

Bao, J., Jana, S. S. and Adelstein, R. S. (2005). Vertebrate nonmuscle myosin II isoforms rescue small interfering RNA-induced defects in COS-7 cell cytokinesis. *J. Biol. Chem.* **280**, 19594-19599.

Berridge, M. J. (1993). Inositol trisphosphate and calcium signalling. *Nature* **361**, 315-325.

Berridge, M. J., Bootman, M. D. and Roderick, H. L. (2003). Calcium signalling: dynamics, homeostasis and remodelling. *Nat. Rev. Mol. Cell Biol.* **4**, 517-529.

Bush, K. T., Stuart, R. O., Li, S. H., Moura, L. A., Sharp, A. H., Ross, C. A. and Nigam, S. K. (1994). Epithelial Inositol 1,4,5-Trisphosphate Receptors. *J. Biol. Chem.* **269**, 23694-23699.

Colosetti, P., Tunwell, R. E., Cruttwell, C., Arsanto, J. P., Mauger, J. P. and Cassio, D. (2003). The type 3 inositol 1,4,5-trisphosphate receptor is concentrated at the tight junction level in polarized MDCK cells. *J. Cell Sci.* **116**, 2791-2803.

Conti, M. A. and Adelstein, R. S. (2008). Nonmuscle myosin II moves in new directions. *J. Cell Sci.* **121**, 11-18.

Cordenonsi, M., D'Atri, F., Hammar, E., Parry, D. A., Kendrick-Jones, J., Shore, D. and Citi, S. (1999). Cingulin contains globular and coiled-coil domains and interacts with ZO-1, ZO-2, ZO-3, and myosin. *J. Cell Biol.* **147**, 1569-1582.

Dufour, J. F., Turner, T. J. and Arias, I. M. (1995). Nitric oxide blocks bile canalicular contraction by inhibiting inositol trisphosphate-dependent calcium mobilization. *Gastroenterology* **108**, 841-849.

Even-Ram, S., Doyle, A. D., Conti, M. A., Matsumoto, K., Adelstein, R. S. and Yamada, K. M. (2007). Myosin IIA regulates cell motility and actomyosin-microtubule crosstalk. *Nat. Cell Biol.* **9**, 299-309.

Farhadifar, R., Röper, J. C., Aigouy, B., Eaton, S. and Jülicher, F. (2007). The influence of cell mechanics, cell-cell interactions, and proliferation on epithelial packing. *Curr. Biol.* **17**, 2095-2104.

Fenteany, G., Janmey, P. A. and Stossel, T. P. (2000). Signaling pathways and cell mechanics involved in wound closure by epithelial cell sheets. *Curr. Biol.* **10**, 831-838.

Fukatsu, K., Bannai, H., Zhang, S., Nakamura, H., Inoue, T. and Mikoshiba, K. (2004). Lateral diffusion of inositol 1,4,5-trisphosphate receptor type 1 is regulated by actin filaments and 4.1N in neuronal dendrites. *J. Biol. Chem.* **279**, 48976-48982.

Glotzer, M. (2005). The molecular requirements for cytokinesis. *Science* **307**, 1735-1739.

Hecht, G., Pestic, L., Nikcevic, G., Koutsouris, A., Tripuraneni, J., Lorimer, D. D., Nowak, G., Guerriero, V. J., Elson, E. L. and Lanerolle, P. D. (1996). Expression of the catalytic domain of myosin light chain kinase increases paracellular permeability. *Am. J. Physiol.* **271**, C1678-C1684.

Hirata, K., Pusl, T., O'Neill, A. F., Dranoff, J. A., Nathanson, M. H. (2002). The type II inositol 1,4,5-trisphosphate receptor can trigger Ca^{2+} waves in rat hepatocytes. *Gastroenterology* **122**, 1088-1100.

Ivanov, A. I., Bachar, M., Babbin, B. A., Adelstein, R. S., Nusrat, A. andParkos, C. A. (2007). A unique role for nonmuscle myosin heavy chain IIA in regulation of epithelial apical junctions. *PLoS ONE.* **2**, e658.

Joseph, S. K., Lin, C., Pierson, S., Thomas, A. P. and Maranto, A. R. (1995). Heteroligomers of type-I and type-III inositol trisphosphate receptors in WB rat liver epithelial cells. *J. Biol. Chem.* **270**, 23310-23316.

Kanada, M., Nagasaki, A. and Uyeda, T. Q. (2005). Adhesion-dependent and contractile ring-independent equatorial furrowing during cytokinesis in mammalian cells. *Mol. Biol. Cell* **16**, 3865-3872.

Kline, C. F., Cunha, S. R., Lowe, J. S., Hund, T. J. and Mohler, P. J. (2008). Revisiting ankyrin-InsP3 receptor interactions: ankyrin-B associates with the cytoplasmic N-terminus of the InsP3 receptor. *J. Cell. Biochem.* **104**, 1244-1253.

Liu, S. L., Fewkes, N., Ricketson, D., Penkert, R. R. and Prehoda, K. E. (2008). Filament-dependent and -independent localization modes of Drosophila non-muscle myosin II. *J. Biol. Chem.* **283**, 380-387.

Maximov, A., Tang, T. S. and Bezprozvanny, I. (2003). Association of the type 1 inositol (1,4,5)-trisphosphate receptor with 4.1N protein in neurons. *Mol. Cell. Neurosci.* **22**, 271-283.

Mikoshiba, K. (1997). The $InsP_3$ receptor and intracellular Ca^{2+} signaling. *Curr. Opin. Neurobiol.* **7**, 339-345.

Mohler, P. J., Davis, J. Q., Davis, L. H., Hoffman, J. A., Michaely, P. and Bennett, V. (2004). Inositol 1,4,5-trisphosphate receptor localization and stability in neonatal cardiomyocytes requires interaction with ankyrin-B. *J. Biol. Chem.* **279**, 12980-12987.

Monkawa, T., Miyawaki, A., Sugiyama, T., Yoneshima, H., Yamamoto-Hino, M., Furuichi, T., Saruta, T., Hasegawa, M. and Mikoshiba, K. (1995). Heterotetrameric complex formation of inositol 1,4,5-trisphosphate receptor subunits. *J. Biol. Chem.* **270**, 14700-14704.

Nobes, C. D. and Hall, A. (1999). Rho GTPases control polarity, protrusion, and adhesion during cell movement. *J. Cell Biol.* **144**, 1235-1244.

Robinson, D. N. and Spudich, J. A. (2004). Mechanics and regulation of cytokinesis. *Curr. Opin. Cell Biol.* **16**, *182-188.*

Sellers, J. R. (2000). Myosins: a diverse superfamily. *Biochim. Biophys. Acta.* **1496**, 3-22.

Shutova, M. S., Alexandrova, A. Y. and Vasiliev, J. M. (2008). Regulation of polarity in cells devoid of actin bundle system after treatment with inhibitors of myosin II activity. *Cell Motil. Cytoskeleton* **65**, 734-746.

Sugiyama, T., Matsuda, Y. and Mikoshiba, K. (2000). Inositol 1,4,5-trisphosphate receptor associated with focal contact cytoskeletal proteins. *FEBS Lett.* **466**, 29-34.

Sutton, T. A., Mang, H. E. and Atkinson, S. J. (2001). Rho-kinase regulates myosin II activation in MDCK cells during recovery after ATP depletion. *Am. J. Physiol.* **281**, F810-F818.

Taylor, C. W., Genazzani, A. A. and Morris, S. A. (1999). Expression of inositol trisphosphate receptors. *Cell Calcium* **26**, 237-251.

Totsukawa, G., Yamakita, Y., Yamashiro, S., Hartshorne, D. J., Sasaki, Y. and Matsumura, F. (2000). Distinct roles of ROCK (Rho kinase) and MLCK in spatial regulation of MLC phosphorylation for assembly of stress fibers and focal adhesions in 3T3 fibroblasts. *J. Cell Biol.* **150**, 797-806.

Tuvia, S., Buhusi, M., Davis, L., Reedy, M. and Bennett, V. (1999). Ankyrin-B is required for intracellular sorting of structurally diverse Ca^{2+} homeostasis proteins. *J. Cell Biol.* **147**, 995-1008.

Walker, D. S., Ly, S., Lockwood, K. C. and Baylis, H. A. (2002). A direct interaction between IP_3 receptors and myosin II regulates IP_3 signaling in C. elegans. *Curr. Biol.* **12**, 951-956.

Wojcikiewicz, R. J. and He, Y. (1995). Type I, II and III inositol 1,4,5-trisphosphate receptor co-immunoprecipitation as evidence for the existence of heterotetrameric receptor complexes. *Biochem. Biophys. Res. Commun.* **213**, 334-341.

Zhang, S., Mizutani, A., Hisatsune, C., Higo, T., Bannai, H., Nakayama, T., Hattori, M. and Mikoshiba, K. (2003). Protein 4.1N is required for translocation of inositol 1,4,5-trisphosphate receptor type 1 to the basolateral membrane domain in polarized Madin-Darby canine kidney cells. *J. Biol. Chem.* **278**, 4048-4056.

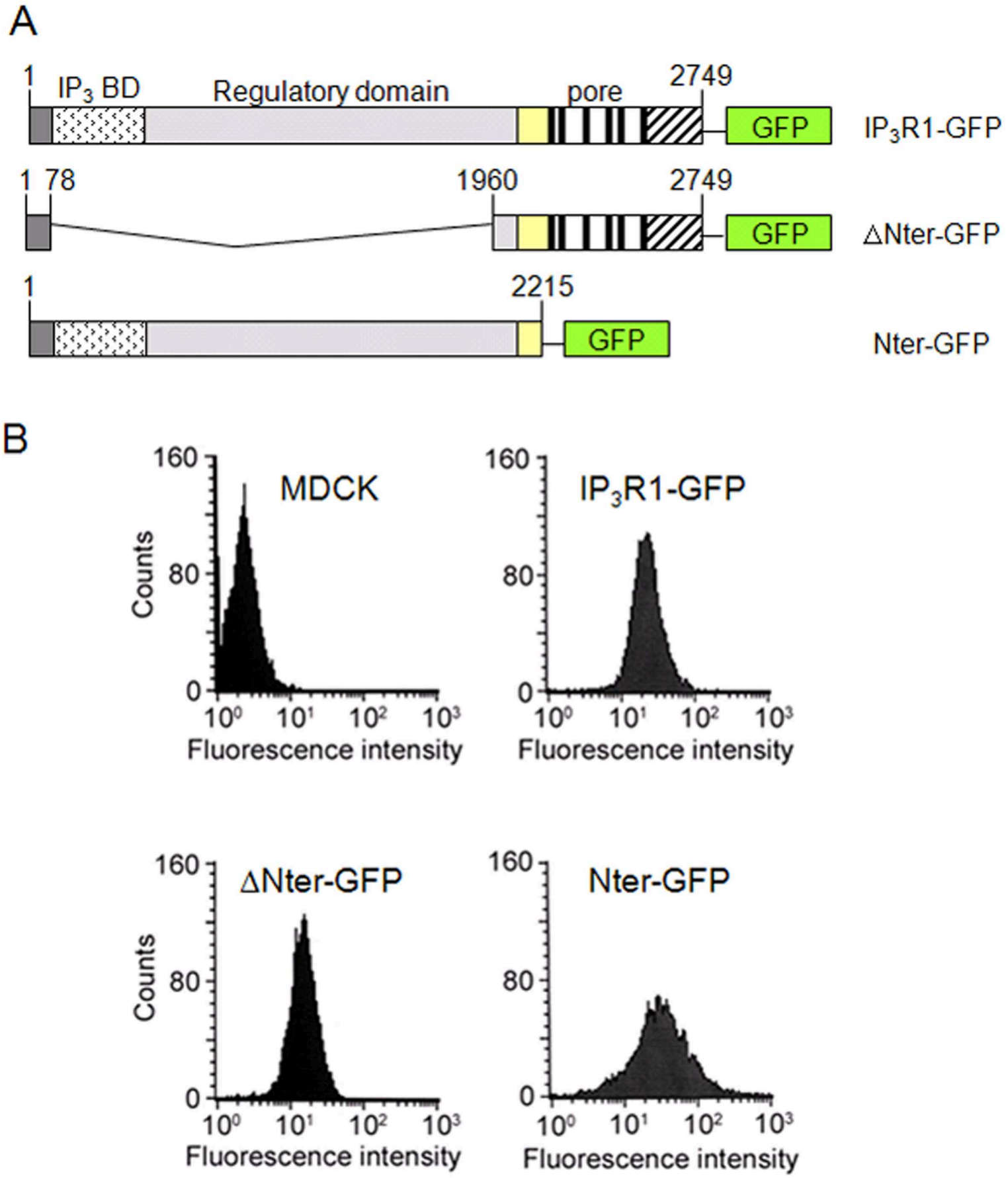

FigureS1: **A :** Schematic representation of the GFP-tagged constructs used in this study. Numbers indicate the amino acids that are still present in the deletion mutants. BD: binding domain **B :** Stable expression of IP3R-GFP, ΔNter-GFP and Nter-GFP in MDCK cells. Transfected cells exhibiting a bright fluorescence were sorted by FACS, expanded and analyzed again after 2 to 3 weeks of cell culture. Non transfected MDCK cells were used as negative controls. Data are presented as histograms of the intensity of fluorescence for each cell population.

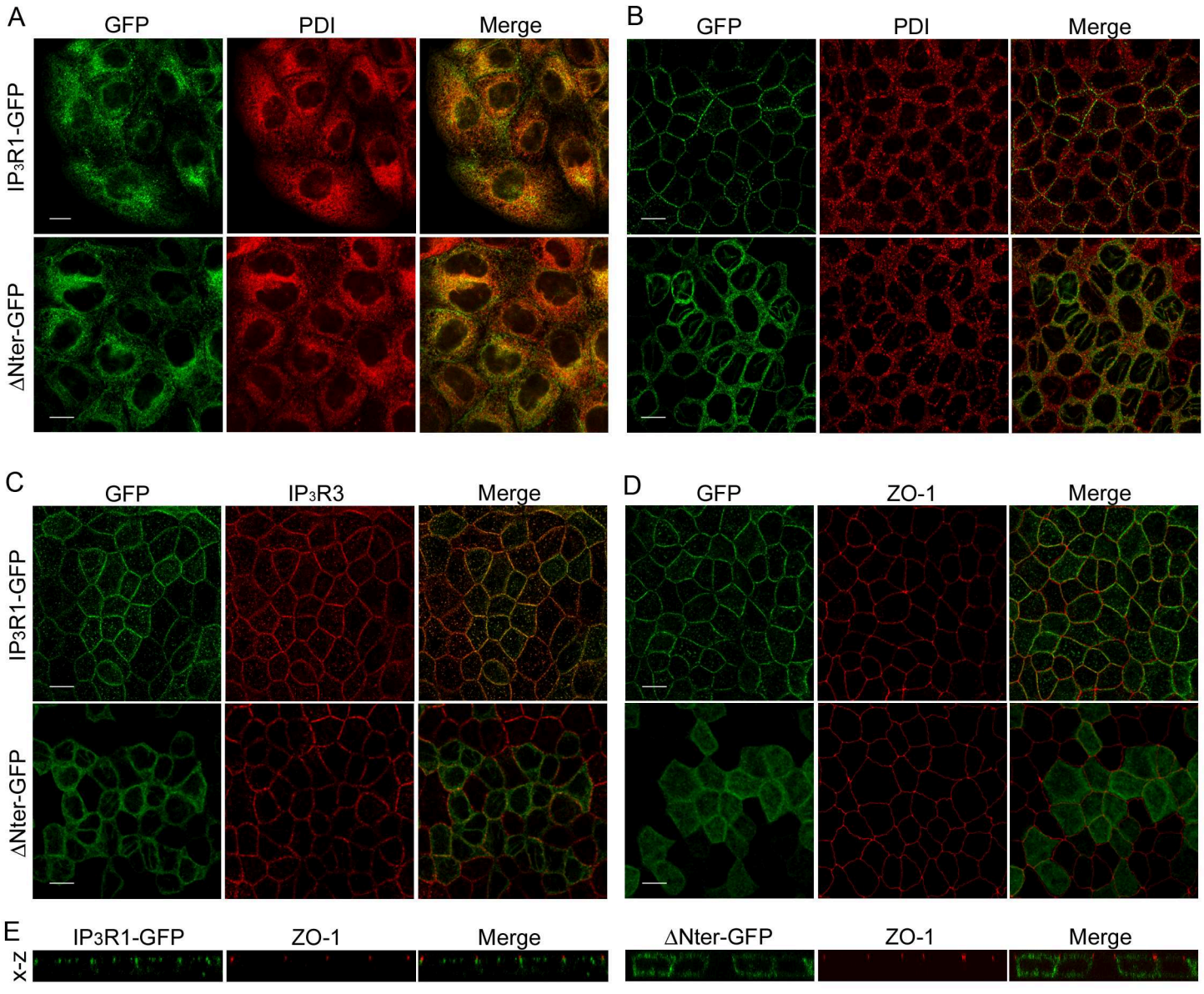

Figure S2: **ΔNter-GFP is still targeted to the ER membrane but does not translocate to the tight junctions as polarity develops. A:** representative x-y confocal sections showing overlapping distribution of IP3R1-GFP or ΔNter-GFP and the ER marker PDI in subconfluent MDCK cells. **B-D:** Representative x-y confocal sections of polarized MDCK cells expressing either IP3R1-GFP or ΔNter-GFP and stained for PDI (B), IP3R3 (C) or ZO-1 (D) demonstrating that, while IP3R1-GFP and endogenous IP3R3 translocate to the cell periphery upon MDCK epithelial cell differentiation, ΔNter-GFP remains evenly distributed in the ER and the nucleoplasmic reticulum. Scale bar, 10 µm. **E:** x-z reconstructions showing that, in contrast to IP3R1-GFP, ΔNter-GFP does not accumulate at the tight junction level as defined by ZO-1 staining in polarized cells. This is likely not due to the saturation of the translocation mechanisms, as endogenous IP3Rs are normally recruited to the apex of the lateral membrane in ΔNter-GFP expressing cells. (x-z), 7,5 µm.

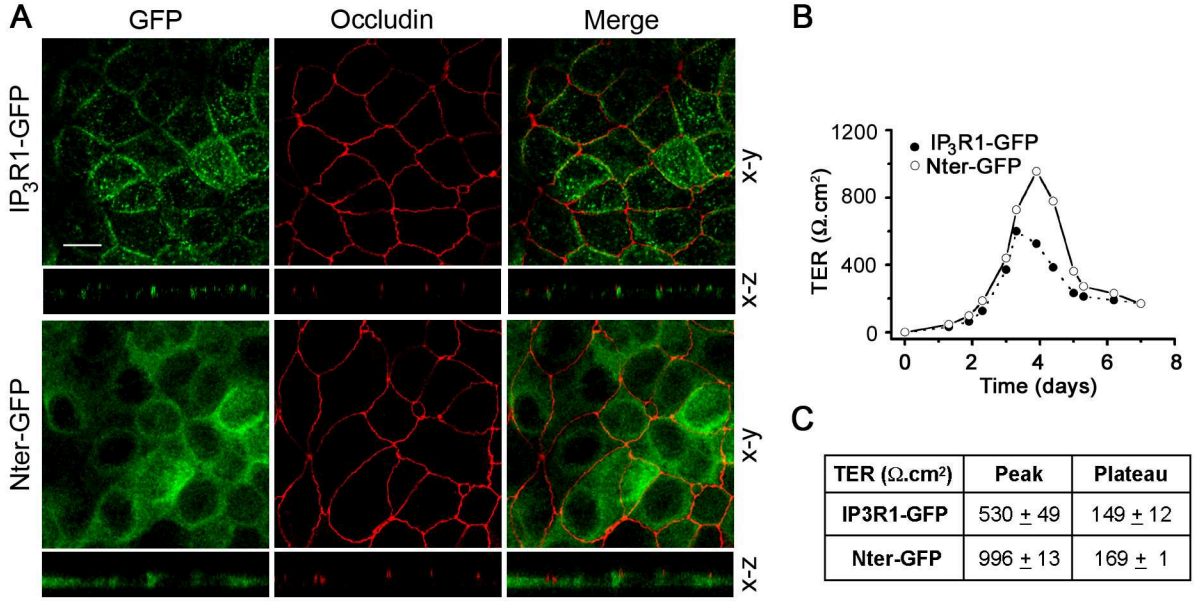

C

TER (Ω.cm²)	Peak	Plateau
IP3R1-GFP	530 ± 49	149 ± 12
Nter-GFP	996 ± 13	169 ± 1

Figure S3: (A) Polarized MDCK cells expressing IP_3R1-GFP or Nter-GFP were fixed, permeabilized, immunostained for occludin and imaged by confocal microscopy. Single confocal x-y sections captured at the TJ level and x-z projections are presented. Scale bar, 10 µm. (x-z), 7.2 µm. **(B)** Representative traces showing the TER development in MDCK cells expressing IP_3R1-GFP (dotted line) or Nter-GFP (solid line) grown on filters (3413, Costar) over a week time period (Initial plating density: 10^4 cells/cm^2) TER was measured at 37°C in culture medium at the indicated time points with a Millicel apparatus (Millipore), and background resistance of empty filters was substracted. **(C)** Average peak and steady-state TER values derived from 3 independent experiments performed in duplicate are given ± s.e.m.

.

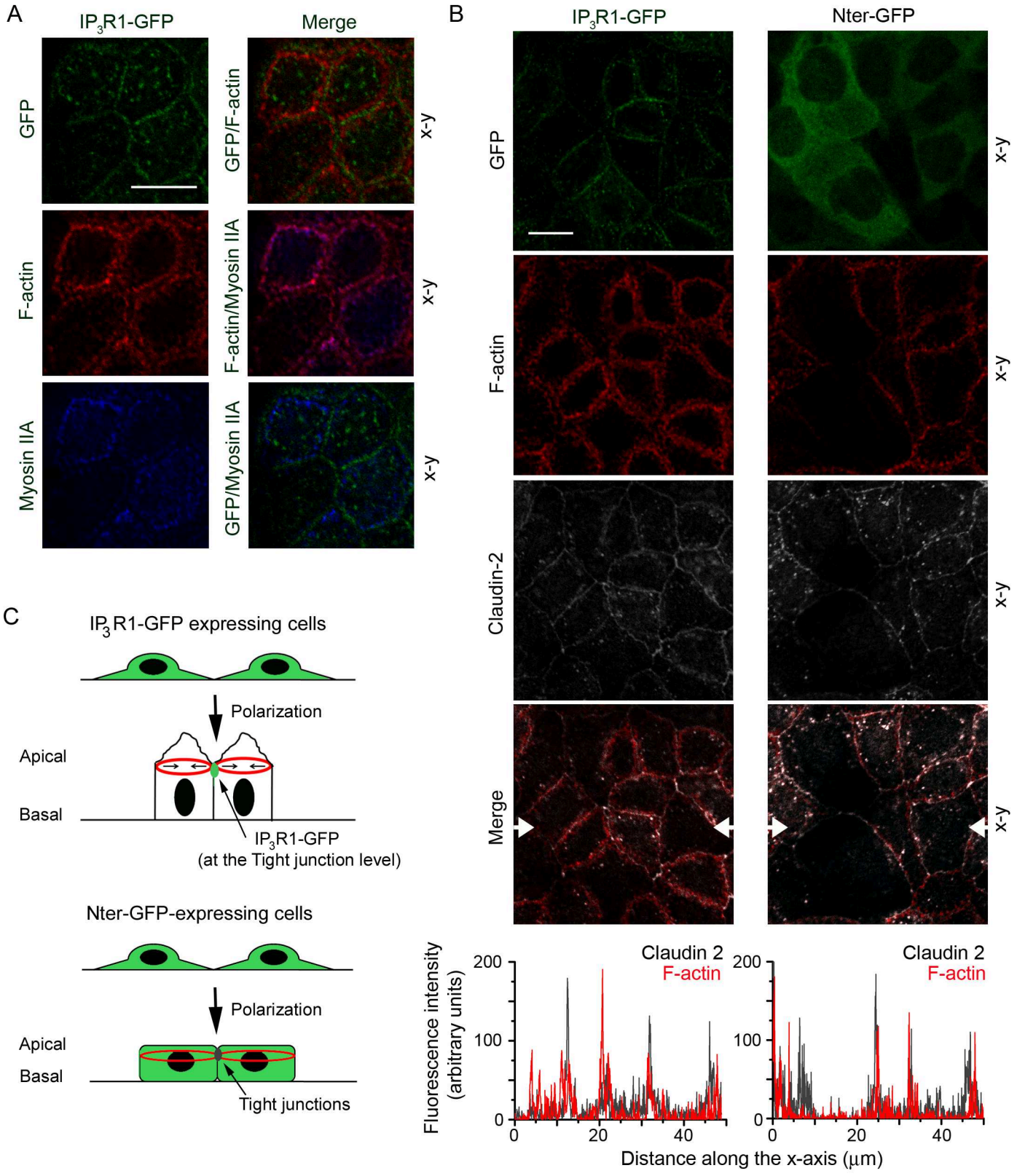

<u>Figure S4:</u> Organization of the perijunctional F-actin belt in IP_3R1-GFP and Nter-GFP cells. **(A)** Polarized MDCK cells expressing IP_3R1-GFP were fixed, permeabilized and double stained for myosin IIA and F-actin. Representative images of myosin IIA and F-actin distribution in individual confocal x-y sections captured at the cell apex are shown. **(B)** Polarized MDCK cells expressing IP_3R1-GFP or Nter-GFP were fixed, permeabilized and double-stained for claudin-2 and F-actin. Single confocal x-y sections captured at the TJ level and intensity profiles of rhodamine-phalloidin and claudin-2 fluorescence obtained along the x axis at the TJ level are presented. Arrows denote positions of the x-z projections Scale bar, 10 µm. **(C)** Schematic illustrating the differences between polarized Nter-GFP and IP_3R1-GFP cells. Red lines illustrate F-actin organization. Arrows represent the centripetal force imposed by myosin IIA on the perijunctional actin belt which contributes to cell compaction.

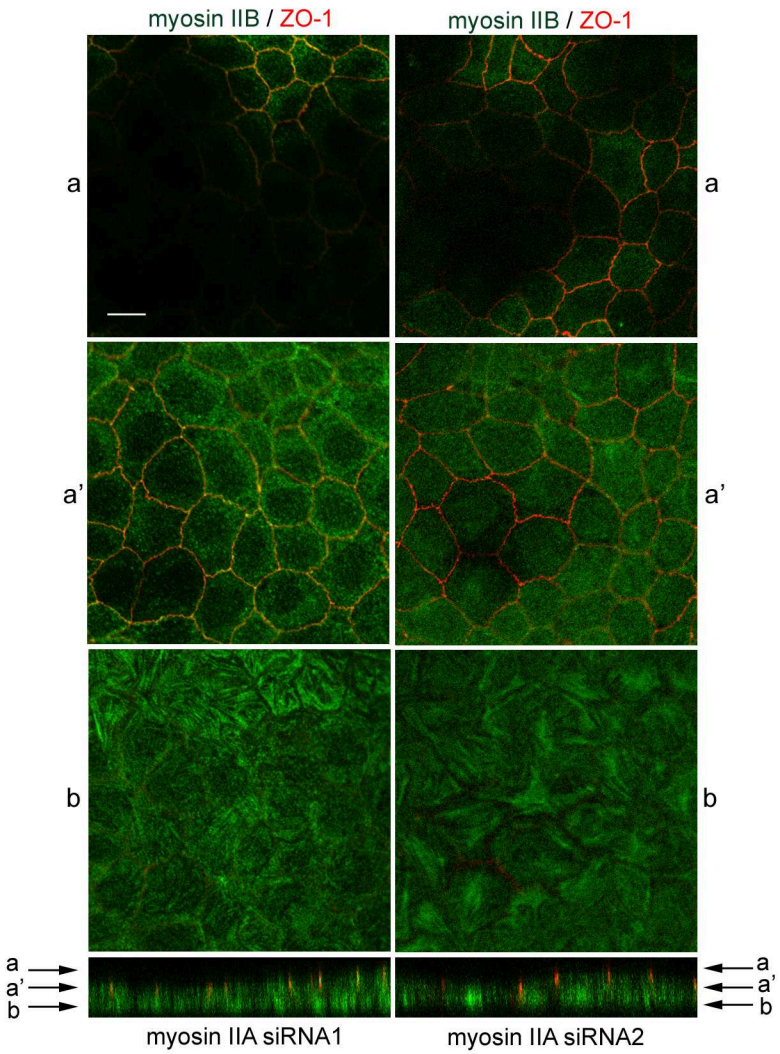

Figure S5: Myosin IIA-targeted siRNAs do not significantly suppress myosin IIB expression. Confluent MDCK cells were transfected with myosin IIA-targeted siRNA1 and on day 3 post-transfection, were fixed and stained for myosin IIB and ZO-1. B: Representative confocal x-y and x-z sections showing that myosin IIB expression was not highly affected even in cells exhibiting the same morphological defects than myosin IIA-depleted cells. Scale bar, 10 μm; (x-z), 8.4 μm.